# Magnetism of $BiFe_{0.9}Cr_{0.1}O_3$ studied experimentally and with Monte Carlo simulations

Jiajun Mo, Puyue Xia, Qinghang Zhang, Haiwen Chen, Lebin Liu, Yanfang Xia,* and Min Liu†
*College of Nuclear Science and Technology, University of South China, Hengyang 421001, China*

(Received 3 September 2021; revised 24 December 2021; accepted 23 February 2022; published 8 March 2022)

The sol-gel technique is used in this paper to prepare Cr-doped $BiFeO_3$. The magnetism of $BiFe_{1-x}Cr_xO_3$ with a distorted rhombohedral perovskite structure has been studied for $x = 0.1$. X-ray diffraction analysis reveals that the sample is rhombohedral with the space group $R_3C$ and contains some impurity phases. The Mössbauer spectra at 300 and 500 K are used to determine the magnetic and impurity phase proportion as well as the valence state, electric field gradient, internal magnetic field, and electron cloud distribution of $Fe^{3+}$ ions in $BiFe_{0.9}Cr_{0.1}O_3$. The magnetic properties of $BiFe_{0.9}Cr_{0.1}O_3$ are complex. Through the zero-field-cooled/field-cooled magnetization curve, the magnetism of $BiFe_{0.9}Cr_{0.1}O_3$ is analyzed. According to the first-order differential of magnetization to temperature, the Néel temperature is determined to be ∼134 K. It is speculated that a partial relaxation structure may exist in the system. Then the Heisenberg model simulation and experimental data are approximated using the particle swarm optimization algorithm to further analyze the magnetism and calculate the more precise phase transformation temperature. It has been determined that the exchange constants for cubic structure and relaxation structure are $J_{\text{Fe-Cr}} = 6.75$ meV, $J_{\text{Fe-Fe}} = -6.13$ meV, $J'_{\text{Fe-Fe}} = -1.16$ meV, and $J'_{\text{Fe-Cr}} = -1.54$ meV. The cubic and relaxation structures contribute 0.71 and 0.29 to magnetism, respectively. According to the Heisenberg model, the Curie temperature should be ∼606 K, and the Néel temperature should be ∼116 K. The ratio of the Curie temperature to the Weiss constant is significantly >5, implying that the entire spin system is in a state of high frustration.

DOI: 10.1103/PhysRevB.105.094411

## I. INTRODUCTION

Multiferroic materials have garnered considerable attention due to their exceptional magnetoelectric properties for ferromagnetism (FM) and ferroelectricity performance. These materials deserve further investigation. $BiFeO_3$ (BFO) is one of multiferroic materials characterized by higher ferroelectric Curie temperature ($T_C = 1103$ K) and antiferromagnetic (AFM) Néel temperature ($T_N = 643$ K) [1], belonging to $ABO_3$. It is a cubic-symmetry ideal structure with the oxygen in the face centers in which the B-site cation (Fe) coordinates sixfold with the octahedron of anions and A-site cation (Bi) coordinates 12-fold with the cuboctahedron of anions [2]. The suppression of the helix spatially spin-modulated structure (SSMS) results in the low magnetic moment of BFO at room temperature. Recently, much literature has reported on the enhancement of magnetic properties caused by doping transition metal elements into the B site to replace Fe of $BiFeO_3$, e.g., Co doping increases the coercive force [3], and Cr doping dramatically increases the saturation magnetization [4,5]. These phenomena are due to transition metal doping destroying the cycloidal structure of the 62 nm [6] incommensurate periodicity helix. In addition, studies indicate that, when $Cr^{3+}$ is doped, the FM superexchange of $Cr^{3+}$-O-$Fe^{3+}$ increases magnetism [7–9]. By using *ab initio* calculations, Song and Liu [10] determined the coupling parameters between $Fe^{3+}$ and $Cr^{3+}$. The superexchange coupling between $Fe^{3+}$ and $Cr^{3+}$ is assumed to be FM; then the Curie temperature is calculated to be ∼450 K by utilizing the Heisenberg model. However, under the *R*3 structure, Baettig *et al.* [11] proposed the $Fe^{3+}$-O-$Cr^{3+}$ AFM exchange theory. $Bi_2FeCrO_6$ has an antiparallel FM configuration since, when the bond angle deviates from a perfect 180°, Cr $t_{2g}$ orbitals and Fe $e_g$ orbitals are mixed. In kinetic superexchange between orbitals, the spin between $Fe^{3+}$ and $Cr^{3+}$ tends to be antiparallel. According to Suchomel *et al.* [12], the lower magnetization of $BiFe_{0.5}Cr_{0.5}O_3$ may result in the formation of Fe- and Cr-rich clusters due to the defect in the B-site cation order. There are numerous $Fe^{3+}$-O-$Fe^{3+}$ and $Cr^{3+}$-O-$Cr^{3+}$ AFM superexchange interactions but only a few $Fe^{3+}$-O-$Cr^{3+}$ FM superexchanges in the system. Simultaneously, the FM interaction between $Fe^{3+}$ and $Cr^{3+}$ prevents this superexchange, resulting in the appearance of a phase transformation point ∼130 K. To a certain extent, each of these has its own unique perspective.

The Heisenberg model is a spin statistical model with more degrees of freedom that accurately describes the coupling between spins. Its theory of exchange interaction plays an important role in the field of magnetism. It can typically describe the magnetic phase transformation, calculate the phase transformation temperature, and more accurately describe the mechanism of magnetism, which is widely used in a variety of fields [10,13]. The mean-field theory is used to fit most magnetic analyses [11]. However, it ignores the thermal fluctuations in the environment and suffers from a certain lack of accuracy that can be avoided by using the Monte Carlo method [13]. With the rapid advancement of computers and

*xiayfusc@126.com
†liuhart@126.com

 

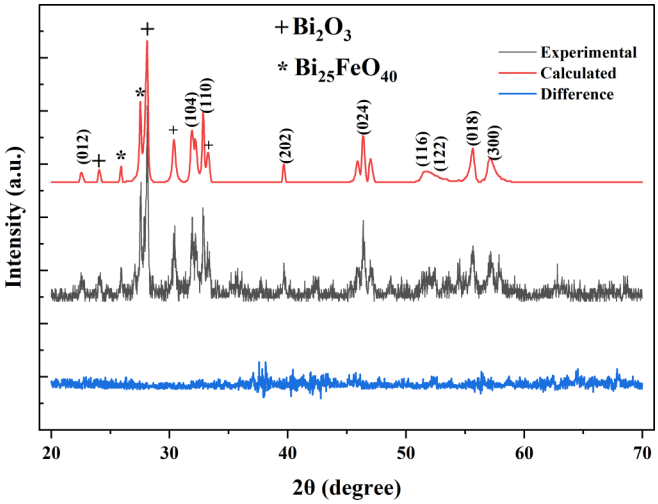


FIG. 1. $BiFe_{0.9}Cr_{0.1}O_3$ x-ray diffraction (XRD) pattern (* indicates the presence of the impurity phase $Bi_2O_3$ [15], and + indicates the presence of the impurity phase $Bi_{25}FeO_{40}$ [16,17]).

the gradual rise of computer simulation, calculated technology based on Monte Carlo can significantly reduce computational complexity, increasing its popularity.

In this paper, we conduct a more in-depth study of $BiFe_{0.9}Cr_{0.1}O_3$, focusing on its magnetism. The composition and magnetic properties of $BiFe_{0.9}Cr_{0.1}O_3$ were analyzed using x-ray diffraction (XRD), Mössbauer spectroscopy, and vibrating sample magnetometry, with the microscopic mechanism simulated by the Heisenberg model. However, during the simulation process, we discover that the material may not be a single-phase molecule but a multiphase molecule, implying that the magnetic composition may contain more than two different interacting lattice contributions to the total magnetism. The magnetism of $BiFe_{0.9}Cr_{0.1}O_3$ is more vividly understood when the classical Heisenberg model is Monte Carlo simulated.

## II. SYNTHESIS OF MATERIAL

The sol-gel method was used to prepare Cr-doped $BiFeO_3$ nanoparticles [14]. All chemicals used were of analytical grade and were not purified further. The sol was prepared by adding $Bi(NO_3)_3$ $5H_2O$ (10.5 mmol), $Cr(NO_3)_3$ $9H_2O$ (1 mmol), and $Fe(NO_3)_3 \cdot 9H_2O$ (9mmol) to ethylene glycol and vigorously stirring for 1 h at 80°C. After that, it was dried for 10 h at 80°C in a drying oven to obtain the brown gel. Finally, the gel was preheated to 400°C and then annealed for 1 h at 550°C to form the $BiCr_{0.1}Fe_{0.9}O_3$ nanoparticles. To compensate for bismuth loss during the annealing process, the sample was prepared with an excess of 5% Bi.

## III. EXPERIMENTAL AND ANALYSIS

### A. Spectroscopic technique

#### *1. XRD*

The structural characterization of $BiFe_{0.9}Cr_{0.1}O_3$ nanometer particles (NPs) using XRD with a Bragg diffraction angle $2\theta$ of between 20° and 80° is shown in Fig. 1. Based on

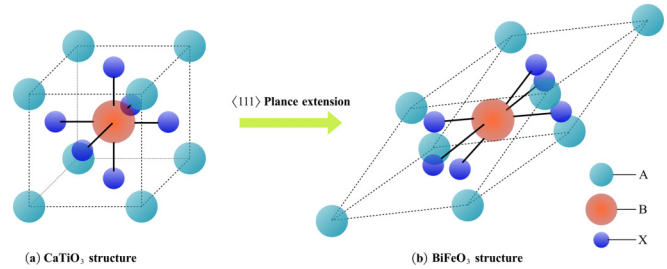


FIG. 2. (a) The typical $CaTiO_3$ structure and (b) the $BiFeO_3$ structure, which transforms from a cubic to a rhombohedral structure along the $ABX_3\langle 111\rangle$ direction.

Bragg's law: $2d\sin\theta = n\lambda$, and we fitted the XRD data using JADE 9.0. It shows that all the peaks indexed as the crystal face (012), (104), (110), (113), (006), (202), (024), and (116) are rhombohedral with the space group $R_3C$ [14,15]. The preparation of $BiFe_{0.9}Cr_{0.1}O_3$ was accompanied by the formation of several impurity phases, including $Bi_2O_3$ and $Bi_{25}FeO_{40}$. According to the XRD spectrum, the $Bi_{25}FeO_{40}$ phase exhibits a strong reflection at a diffraction angle of 28.1°. This is due to the formation of kinetic impurity phases during synthesis [18,19]. The perovskite structure and directional distortion of $ABX_3\langle 111\rangle$ are depicted in Fig. 2. The lattice constants are $a = b = 5.578$ Å, $c = 13.892$ Å, and the cell volume is 373.44 Å$^3$. The crystallite size $D$ is calculated to be 40.8 ± 2 nm using the Scherrer equation ($D = k\lambda/\beta\cos\theta$), where $\lambda$ is the x-ray wavelength, $\beta$ represents the half peak width, and $k$ is a constant distribution with a value of 0.89.

#### *2. Mössbauer spectra*

Here, $^{57}$Fe Mössbauer spectroscopy is a precise method for studying the charge distribution around iron atoms. It was performed at temperatures of 300 and 500 K on $BiFe_{0.9}Cr_{0.1}O_3$ using a conventional 45 mCi $^{57}$Co source steady-acceleration spectrometer at room temperature, and MÖSSWIN4.0 software was used to fit parameters such as isomer shifts (ISs), quadrupole splitting (QS), and hyperfine field. Figure 3 shows the spectra of $BiFe_{0.9}Cr_{0.1}O_3$ NPs at temperatures of 300 and 500 K. These spectra are highly symmetrical, indicating that the spiral rotation of magnetic moments in $BiFe_{0.9}Cr_{0.1}O_3$ has been destroyed [20]. The optimal results are obtained by combining two sextets and a doublet. All parameters are rendered in Table I. The existence of the doublet indicates that the charge surrounding the nucleus of the atom has an asymmetric magnetic moment alignment and is subjected to a specific electric field gradient. The phase represented by the doublet is most likely to correspond to the paramagnetic impurity phase $Bi_{25}FeO_{40}$ [4,14,21], which also confirms the presence of a single iron-containing impurity, e.g., $Bi_{25}FeO_{40}$, as revealed by the XRD analysis process. This paramagnetic impurity accounts for only 4.2 or 5.3% of the Mössbauer spectra and is paramagnetic at 300 and 500 K, which is insufficient to provide enormous magnetism. Therefore, impurities will have no effect on the magnetism measured at room temperature. This slight difference is due to the deviation caused by the low absorptivity of the Mössbauer spectrum in the high-temperature (500 K) region. The Fe valence state of the entire

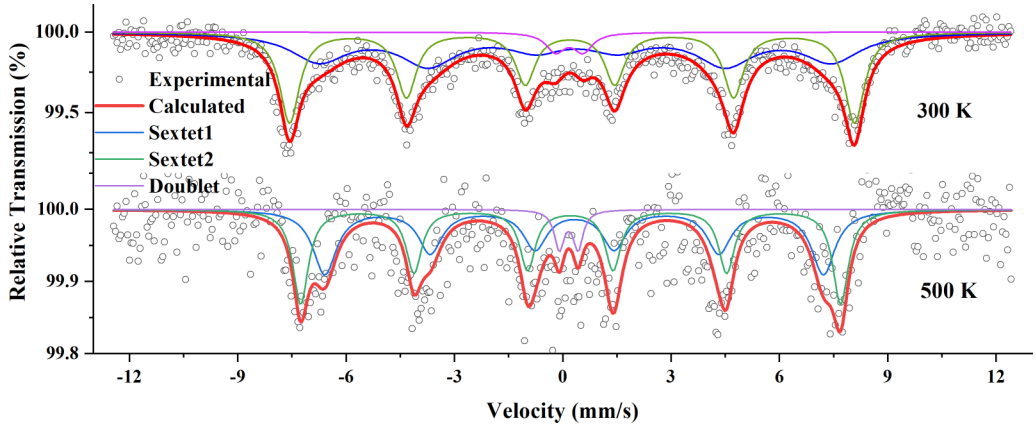


FIG. 3. $^{57}$Fe Mössbauer spectra of $BiFe_{0.9}Cr_{0.1}O_3$ at 300 and 500 K. The red line represents the total fitting curve. Blue and green lines are the sextets with the hyperfine fields, while the purple line denotes a paramagnetic doublet.

sample can be determined to be +3 valence with high spin from the IS of two sextets, and the Fe ions with +2 or +4 valences can be ruled out [22]. The QS of sextet1 exhibits a small negative value attributed to the cubic structure of the sample [23]. Additionally, it exhibits antiparallel ordering between magnetic moments of two magnetic atoms. The positive QS of sextet1 represents weak FM [14]. The larger linewidth at 300 K may be due to the modulation of hyperfine energy produced by the rotation of the magnetic moment relative to the *c* axis of the crystal [23]. However, it is worth noting that the internal Zeeman hyperfine field of sextet1 is only 44.13 T at 300 K, significantly weaker than the 48.64 T hyperfine field of sextet2. The same is true for 500 K, which is caused by the destruction of SSMS [24,25] when Cr is used to replace 10% of the iron sites [24,26]. The hyperfine field at 500 K is only slightly weaker than that of 300 K, indicating that the magnetism of $BiFe_{0.9}Cr_{0.1}O_3$ is still quite strong at 500 K, i.e., the Curie temperature of $BiFe_{0.9}Cr_{0.1}O_3$ is much higher than 500 K.

### B. Magnetic measurements

Field-cooled (FC) and zero-field-cooled (ZFC) measurements were made at a magnetic field strength of 100 Oe and temperatures ranging from 5 to 400 K. The sample was cooled to 5 K at zero field and measured under 100 Oe with increasing temperature. The temperature-dependent magnetization with FC and ZFC is shown in Fig. 4. There is an apparent bifurcation phenomenon, which is characteristic of spin-glass states. The spin-glass behavior is caused primarily by magnetic anisotropy, deformed lattices, and random occupation of magnetic ions [27], but it can also be caused by competition between FM and AFM interactions. However, when a 100 Oe weak magnetic field is applied, the magnetization changes significantly at low temperatures, ruling out the possibility of the sample being locked due to high magnetic anisotropy. Moreover, there is a strong bifurcation trend at 400 K, and the slope of the ZFC/FC magnetization curves is not equal. It indicates that the freezing temperature $T_f$ is $> 400$ K. In other words, the entire test procedure is kept below the freezing temperature.

As the temperature decreases, the field no longer constrains the spin orientation, the heat disturbance energy gradually decreases, the spin direction tends to be ordered, and the magnetization tends to zero. It also exhibits a clear trend of thermal growth $<\sim$14 K, simultaneously. According to the Goodenough-Kanamori rules [28] and Anderson's theory [29], the high-spin $Fe^{3+}(e_g)$-O-$Fe^{3+}(e_g)$ may be more prone to AFM superexchange, and thus, the magnetization tending to zero can be attributed to AFM superexchange dominated by $Fe^{3+}$-O-$Fe^{3+}$. It is worth noting that numerous reports refer to $Fe^{3+}$-O-$Cr^{3+}$ FM coupling [9]. However, in terms of the overall curve pattern of magnetization, there is a peak value of magnetization during temperature changes, which is typically caused by the thermal dependence of two or more sublattices in a ferrimagnetic system. The ferrimagnetism is probably caused by the magnetic moment of different magnetic moments of $Fe^{3+}$ and $Cr^{3+}$. Thus, the possibility exists that $Fe^{3+}$-O-$Cr^{3+}$ is AFM coupling interaction. Given the low content of $Cr^{3+}$, this weak FM does not appear to be strongly

TABLE I. Mössbauer spectral parameters for $BiFe_{0.9}Cr_{0.1}O_3$ NPs at 300 and 500 K.

| Temperature | | IS (mm/s) | QS (mm/s) | Hyperfine field (T) | Area (%) | Valence state |
|---|---|---|---|---|---|---|
| 300 K | Sextet1 | 0.24 ± 0.01 | 0.06 ± 0.01 | 48.64 ± 0.07 | 47.2 | $Fe^{III}$ high spin |
| | Sextet2 | 0.38 ± 0.04 | −0.03 ± 0.07 | 44.13 ± 0.79 | 48.6 | $Fe^{III}$ high spin |
| | Double | 0.19 ± 0.05 | 0.76 ± 0.09 | – | 4.2 | $Fe^{III}$ low spin |
| 500 K | Sextet1 | 0.21 ± 0.02 | 0.01 ± 0.06 | 46.47 ± 0.21 | 47.1 | $Fe^{III}$ high spin |
| | Sextet2 | 0.32 ± 0.04 | −0.01 ± 0.04 | 42.90 ± 0.46 | 47.6 | $Fe^{III}$ high spin |
| | Double | 0.17 ± 0.07 | 0.52 ± 0.10 | – | 5.3 | $Fe^{III}$ low spin |

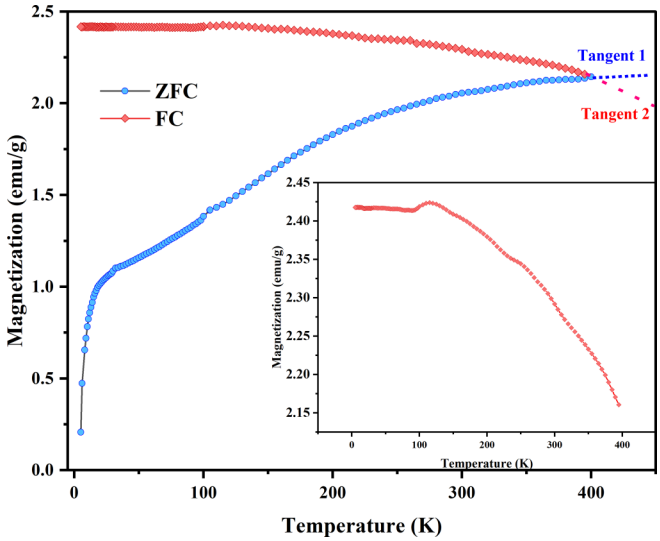


FIG. 4. The field-cooled (FC) and zero-field-cooled (ZFC) *M*-*T* curves of $BiFe_{0.9}Cr_{0.1}O_3$. The slope of tangent line 1 is $\frac{dM_{ZFC}}{dT}|_{T=400\ K}$, and the slope of tangent 2 is $\frac{dM_{FC}}{dT}|_{T=400\ K}$. The inset shows the plot of FC as a function of temperature.

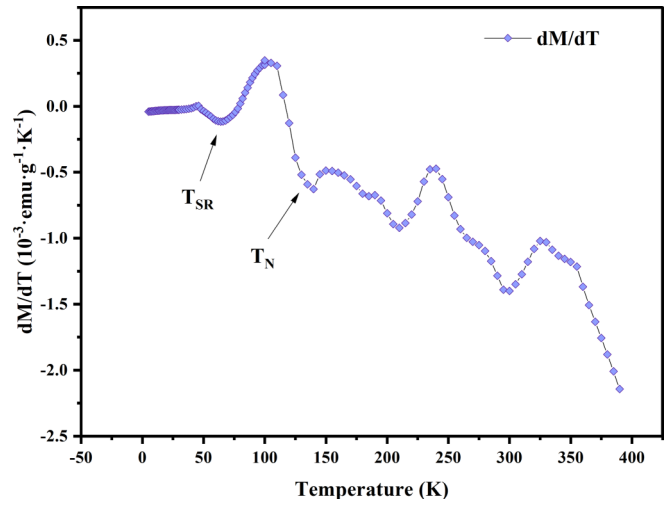


FIG. 5. The first derivative of the field-cooled magnetization curve concerning temperature.

reflected in macroscopic magnetism, and the specific coupling form of $Fe^{3+}$-O-$Cr^{3+}$ will be described in Sec. IV C. The ZFC curve continues to exhibit an upward trend as the temperature increases, indicating that the whole system is dominated by AFM at low temperatures.

The FC magnetization generally shows a downward trend. Additionally, when the FC magnetization range is restricted to a small range (2.15–2.45 emu/g), the cold-field magnetization is relatively stable with temperature change when the temperature is <114 K. At 114 K, maximum magnetization is frequently referred to as a spin-reorientation transformation [30,31]. The magnetization dependence on temperature is like *p*-type Néel ferrimagnetism [32], which can be explained by the magnetization of the sublattice having a different temperature dependence, and the temperature corresponding to the maximum is the Néel temperature $T_N$. This will be confirmed further in the following theoretical study.

Generally, the first-order differential of temperature can be used to calculate the transformation temperature $T_N$ and the spin redirection temperature point $T_{SR}$. Magnetization vs temperature is depicted in Fig. 5 as a first-order differential curve. In conjunction with Fig. 4, the first two minimum points correspond to $T_{SR}$ and $T_N$, respectively. Here, $T_{SR}$ denotes the transformation from AFM to weak FM or ferrimagnetic states through spin redirection, and $T_N$ is the Néel temperature ∼134 K, which is typically used to denote the transformation process from paramagnetic to AFM states. From Fig. 4, there are four minimum temperatures. Apart from the first two, the remaining minimum temperature may be caused by magnetic disorder impurities. Additionally, the minimum appears when the highest temperature reaches 400 K, indicating that the phase transformation temperature may persist beyond 400 K. The phase transformation temperature may be caused by the angle tilt of $Fe^{3+}$-O-$Fe^{3+}$ which prevents the magnetic moment from completely canceling out. That is, the antisymmetric anisotropy caused by Dzyaloshinsky-Moriya (DM) interaction [33,34], confers on the system weak FM. The Hamiltonian form of DM interaction is commonly denoted by the symbol $\mathbf{D} \cdot [\mathbf{S}_i \times \mathbf{S}_j]$, and $\mathbf{D}$ is the DM interaction parameters. The cross product between $\mathbf{S}_i$ and $\mathbf{S}_j$ indicates that it is vertically inclined, resulting in the formation of a canting moment.

The magnetization function with respect to the magnetic field is shown in Fig. 6. The magnetization was measured under an external magnetic field ranging from −70 to 70 kOe. As illustrated, the coercivity of the sample $H_C$ is low, indicating that the material is still in an AFM state at 300 K. Notably, the magnetization approaches saturation, and the $M_S$ value is ∼13.0 emu/*g*. This high magnetization indicates that the spatially modulated spin cycloid has no discernible effect on the internal structure of $BiFeO_3$. The following possibilities are inferred from this high-saturation magnetization: To

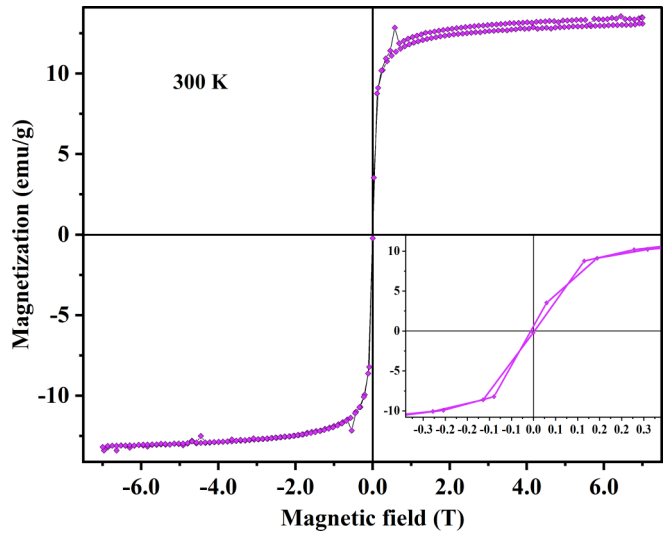


FIG. 6. The magnetization (*M*-*H*) for the sample of $BiFe_{0.9}Cr_{0.1}O_3$ at 300 K. The inset shows an enlarged view in the vicinity of the origin of the coordinates.

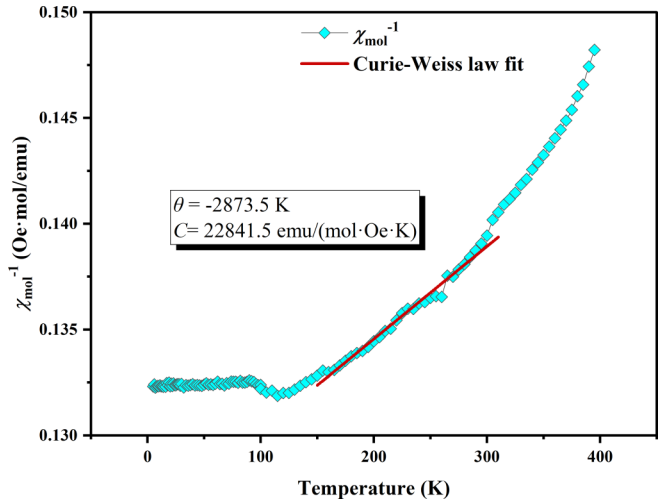


FIG. 7. The reciprocal of molar susceptibility ($\chi_{mol} = \frac{M_{mol}}{H}$) varying with temperature from 5 to 400 K. The red line is the fitted curve with the Curie-Wiess law.

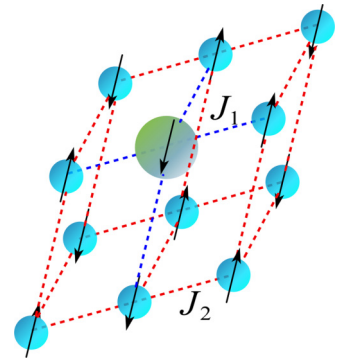


FIG. 8. The magnetic exchange structure diagram of the atomic lattice arrangement, where blue represents Fe, and cyan represents Cr. The size of the ball is only for apparency and has no practical significance. Among them, the oxygen atom, which serves as the medium of exchange between the two atoms, is ignored.

begin, this material is reduced to a nanometer size, which destroys the helical structure with a periodicity of 62 nm and suppresses the AFM order of (111) FM planes, achieving the magnetic enhancement effect [11,35]. Secondly, lattice distortion would introduce a small amount of $Fe^{2+}$ ions, and $Fe^{2+}$-O-$Fe^{3+}$ forms FM which increases magnetism, but this guess does not appear to be valid based on Mössbauer spectral results; the system contains no $Fe^{2+}$ ions. Thirdly, because the radius of $Cr^{3+}$ ion is smaller than that of the $Fe^{3+}$ ion when $Cr^{3+}$ is doped into the lattice, it induces a specific lattice strain and forms a certain tilt angle. As a result, the magnetic moment of the AFM action of $Fe^{3+}$-O-$Fe^{3+}$ cannot be offset, resulting in ferrimagnetism. Finally, due to sufficient stirring, the components of each phase are randomly and uniformly distributed, which may result in some structural damage and lattice strain. Simultaneously, impurities introduced during the preparation process can significantly destroy the spiral structure, which releases the magnetism and significantly improves the magnetism, as is also reflected in Ref. [36]. The ferrimagnetism configuration described above is indeed the ground state, and there is no cancellation of the macroscopic magnetization; rather, it results in a significant increase in magnetism.

The Weiss constant $\theta$ and Curie constant $C$ are determined by linear fitting of the reciprocal magnetic susceptibility $\chi_{mol}^{-1}$ using the Curie-Wiess formula $\chi_{mol} = \frac{C}{T-\theta}$. Figure 7 illustrates the fitting results of $\chi_{mol}^{-1}$ between 150 and 300 K. The result shows that $\theta = -2873.5\,\mathrm{K}$ and $C = 22841.5\,\mathrm{emu/(mol\,Oe\,K)}$. The enormous negative $\theta$ corresponds to the paramagnetic Curie temperature, indicating that the system exhibits a high degree of AFM interaction.

## IV. MODELS AND CALCULATION METHODS

### A. Establishment of classical Heisenberg model

Given that $BiFeO_3$ is a G-type AFM structure, AFM exchange occurs in the nearest-neighbor coupling of $Fe^{3+}$-O-$Fe^{3+}$. When the $Cr^{3+}$ ion concentration is increased, the overall superexchange system remains unchanged, and most of the literature reported FM coupling in $Fe^{3+}$-O-$Cr^{3+}$ [7–9]. However, the Cr-doped process may result in Jahn-Teller distortion and orbital ordering effect, which will lead to AFM in one direction and FM coupling in the other direction [11]. When the bond angle of $Fe^{3+}$-O-$Cr^{3+}$ is $<180°$, the cubic structure transforms into a relaxed structure, resulting in AFM coupling between the $Fe^{3+}$ and $Cr^{3+}$. Due to the destruction of the helical structure, the magnetic contribution of each cell is well reflected in the macroscopic magnetism. Accordingly, it is worth considering using the Heisenberg model to study and analyze the magnetism of a single crystal cell, while coupling action is used to investigate the cause of magnetism.

We analyze the magnetism of $BiFe_{0.9}Cr_{0.1}O_3$ by establishing a classical Heisenberg model and fitting experimental data to calculate the exchange-coupling constant of $BiFe_{0.9}Cr_{0.1}O_3$. The Hamiltonian of the system is given by

$$\mathcal{H} = -\sum_{\langle i,j\rangle} J_{ij}\mathbf{S}_i \times \mathbf{S}_j - \sum_i \mathbf{H} \times \boldsymbol{S_i} - K\sum_i S_i^{z^2}, \quad (1)$$

where $\mathbf{S}_i$ is the spin vector at site $i$, which represents the pseudospins of Cr and Fe ($S_{Cr} = \frac{3}{2}$, $S_{Fe} = \frac{5}{2}$, respectively), and $\langle i,j\rangle$ denotes distinct pairs of nearest-neighbor sites. The intensity of exchange coupling between two points can be expressed using the coupling constants $J_{ij}$. Here, $\mathbf{H}$ is the vector of the external magnetic field. To be as consistent as possible with the experimental results, $\mathbf{H}$ is defined in this paper as the transverse field in the $x$-axis direction with the field strength of 100 Oe. Also, $K$ denotes an anisotropic constant, and $S^z$ represents the spin component along the $z$ axis.

Because the double perovskite structure of $Bi_2FeCrO_6$ often resembles the crystal structure of sodium chloride, the chessboard distribution of $Fe^{3+}$ and $Cr^{3+}$ randomly places the Cr in the Fe site, avoiding $Cr^{3+}$-O-$Cr^{3+}$ nearest exchange coupling. Figure 8 illustrates a simplified lattice schematically. As seen from the diagram, the interaction preceding each B site can be treated ignoring the lattice distortion. The layout structure of $BiFe_{0.9}Cr_{0.1}O_3$ is shown in Fig. 9. During the simulation, each magnetic atom must be placed

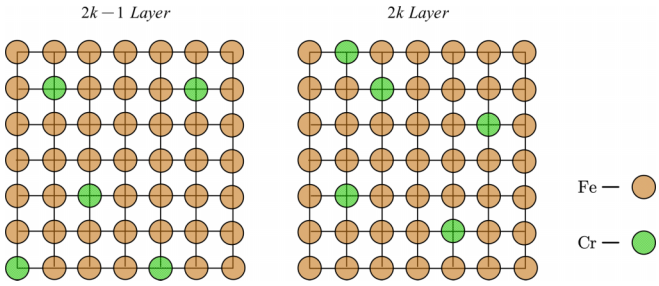


FIG. 9. Different layer structures of $BiFe_{0.1}Cr_{0.9}O_3$, where the green and brown balls represent Fe and Cr atoms, respectively. The atoms are randomly arranged on the chessboard lattice.

in layers, the Cr atoms must be randomly distributed, and periodic boundary conditions can be used to minimize boundary effects. Although some distortions exist in the structure of $BiFe_{0.9}Cr_{0.1}O_3$, the O and Bi atoms can be ignored in magnetic simulations and the lattice structure of magnetic exchange studied.

### B. Monte Carlo method

The entire simulation process is carried out using the Metropolis Hasting Algorithm. Each loop traversal is referred to as one Monte Carlo step (MCS). With $10^4$ MCS for evolution and $10^5$ MCS for the statistical simulation of the Heisenberg model. Each MCS loop flips all atoms, with a flip probability $p$ of

$$p = \exp\left(-\frac{\Delta H}{k_B T}\right), \tag{2}$$

where $\Delta H$ denotes the energy difference between the preflip and postflip states, $T$ is the temperature, and $k_B$ is Boltzmann constant. The following can be calculated using this algorithm: magnetization, magnetic susceptibility, heat capacity, and Curie temperature.

Magnetization is defined by the average value of all spins:

$$M = \frac{\sum_{i=1}^{L^3} S_i}{N}, \tag{3}$$

where $N = L \times L \times L$, and $L$ is the number of magnetic atoms on the edge of a cubic lattice; the magnetic properties are usually well reflected when $L$ is 20, but the range of change is more fragile when $L$ is more significant [13].

Magnetic susceptibility can be used to characterize the phase transformation temperature and is typically determined by deducing approximate statistics. It can be calculated by

$$\chi = \frac{\partial M}{\partial H} = \frac{N(\Delta M)^2}{k_B T} = N\frac{\langle M^2\rangle - \langle M\rangle^2}{k_B T}. \tag{4}$$

Initially, the exchange constants $J_{\text{Fe-Cr}}$ and $J_{\text{Fe-Fe}}$ are calculated using the fitting method, the standardized data $F$ are approximated using the particle swarm optimization (PSO) algorithm, and the fitness function is the sum of squares of residuals. The standardized data $F$ is

$$F = \frac{M - \min M}{\max M - \min M}. \tag{5}$$

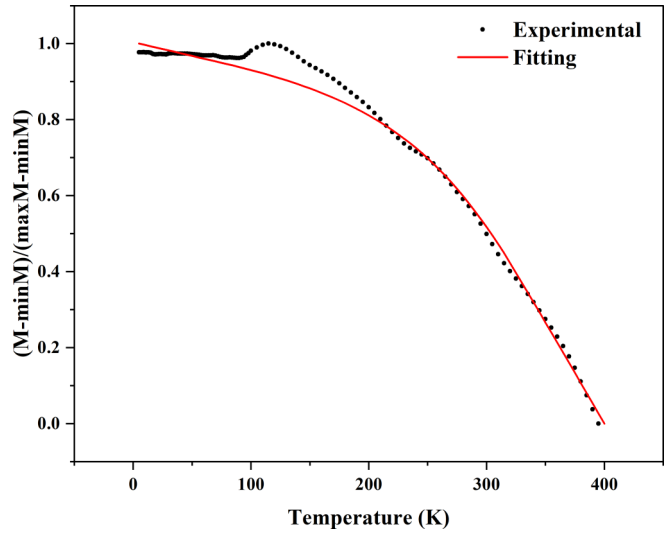


FIG. 10. Fitted results for a single phase with ferromagnetic (FM) superexchange between $Fe^{3+}$ and $Cr^{3+}$.

Here, $M$ is the unprocessed magnetization array (arbitrary unit), min$M$ represents the minimum of array $M$, and max$M$ denotes the maximum of array $M$.

### C. Calculation process and results

We attempted but failed to fit the experimental data based on the FM superexchange between $Fe^{3+}$ and $Cr^{3+}$. The fitted result is shown in Fig. 10. Through the fitting, an unphysical anisotropy parameter $K \sim 36.3$ meV is obtained, noting that the system exhibits significant anisotropy, which deviates from the actual situation. Moreover, regardless of how the parameters are adjusted, the magnetization curve will never exhibit a rise ∼114 K. This is because, when $Fe^{3+}$ and $Cr^{3+}$ are FM superexchanged and $Cr^{3+}$ occupies the same sublattice, the sites containing $Cr^{3+}$ in the sublattice of $Cr^{3+}$ are parallel to the spin of the sublattice of the surrounding $Fe^{3+}$, the magnetic moment is superimposed, and the magnetization gradually decreases as the temperature increases, following the magnetization behavior of a typical FM, i.e., magnetization and temperature have a strictly decreasing relationship.

One possibility is that the $BiFe_{0.9}Cr_{0.1}O_3$ contains a partial relaxation structure that results in the AFM coupling of

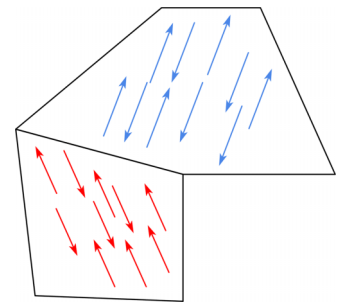

FIG. 11. The distribution of magnetic domains with different structures, in which the blue and red arrows correspond to the spin directions of magnetic atoms with the relaxation structure and the cubic one, respectively.

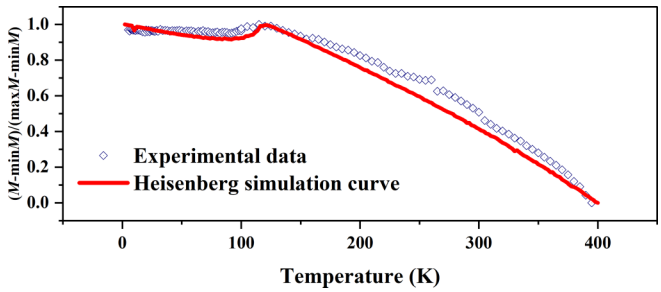


FIG. 12. The magnetization simulated by the classical Heisenberg model compared with the experimental data. The results are normalized and standardized dimensionless data.

the $Fe^{3+}$-O-$Cr^{3+}$. Kazan *et al.* [29] discovered that magnetic phases coexist in the double perovskite structure, i.e., there are at least two magnetic phases. Nechache *et al.* [37] investigated the double-perovskite structure of $Bi_2FeCrO_6$ and held that the system possessed both FM and AFM. The magnetic analysis presented in this paper indicated that the system probably contained at least two magnetic phases. As a result, it was postulated that a system could exist with cubic and relaxation structures coexisting. We fitted the experimental data using the Heisenberg model based on this assumption. The relaxation and cubic structures are divided into two lattices, with the assumption that the two lattices are self-contained. The final proportional distribution of each lattice is fitted using experimental data. This is accomplished by treating the relaxation structure and the cubic structure as two separate clusters, as illustrated in Fig. 11, and calculating their proportions to accurately describe the structure in the macroscopic level. It is possible to obtain a proportional relationship between the relaxation structure and the cubic one.

#### *1. Intelligent search for the most suitable Heisenberg model simulation parameters with PSO algorithm*

Table II shows the fitting parameters, i.e., the exchange constant under cubic structure $J_{\text{Fe-Cr}} = 6.75\,\text{meV}$, $J_{\text{Fe-Fe}} = -6.13\,\text{meV}$, the exchange constant under relaxation structure $J'_{\text{Fe-Fe}} = -1.16\,\text{meV}$ and $J'_{\text{Fe-Cr}} = -1.54\,\text{meV}$. The repulsive potential energies $U$ of $J_{\text{Fe-Fe}}$ and $J'_{\text{Fe-Cr}}$ are 4.6 and 5.5 meV, respectively [11]. Additionally, the value of $J_{\text{Fe-Cr}}$ is nearly identical to that of $J_{\text{Fe-Cr}}$ in Ref. [10]. Figure 12 shows a magnetization curve simulated by two coexisting structures based on their weights, with the relaxation structure and cubic one having weights of 0.29 and 0.71, respectively. Because the symbols of $J_{\text{Fe-Cr}}$ and $J'_{\text{Fe-Cr}}$ are diametrically opposite, their macroscopic magnetic moments should be opposed in theory, and thus, their total magnetization equals the difference between their magnetizations. In addition, the fitting results indicate that the anisotropy cubic structure $K_1$ and the relaxation structure $K_2$ parameters are $K_1 = 0.23\,\text{meV}$ and $K_2 = 3.79\,\mu\text{eV}$, respectively. The Heisenberg model fits the shape of the data in general, but because the classical Heisenberg model is ideal and ignores numerous phenomena such as DM interaction, Jahn-Teller effect, and spin-orbit coupling, the fitted results are slightly different from the actual results. The Heisenberg model accurately describes the temperature at which the phase transformation occurs. Thus, the magnetic susceptibility can be used to determine the Curie and Néel temperatures more precisely. Figure 13 shows the susceptibility and magnetization curves at temperatures ranging from 0 to 800 K. The precise Néel temperature $T_N$ is 116 K, and the precise Curie temperature $T_C$ is ~606 K. The predicted magnetization curve clearly demonstrates phase transformation of magnetization.

TABLE II. Heisenberg simulation fitting parameters under two structures. $J_{\text{Fe-Cr}}$ and $J_{\text{Fe-Fe}}$ represent $Fe^{3+}$-O-$Cr^{3+}$ and $Fe^{3+}$-O-$Fe^{3+}$ superexchanges, $K$ is an anisotropic parameter, and $\omega$ is the magnetic contribution ratio of the two structures.

| | $J_{\text{Fe-Cr}}$ (meV) | $J_{\text{Fe-Fe}}$ (meV) | $K$ ($\mu$eV) | $\omega$ (%) |
|---|---|---|---|---|
| Cubic structure | 6.75 | −6.13 | 230 | 71 |
| Relaxation structure | −1.54 | −1.16 | 3.79 | 29 |

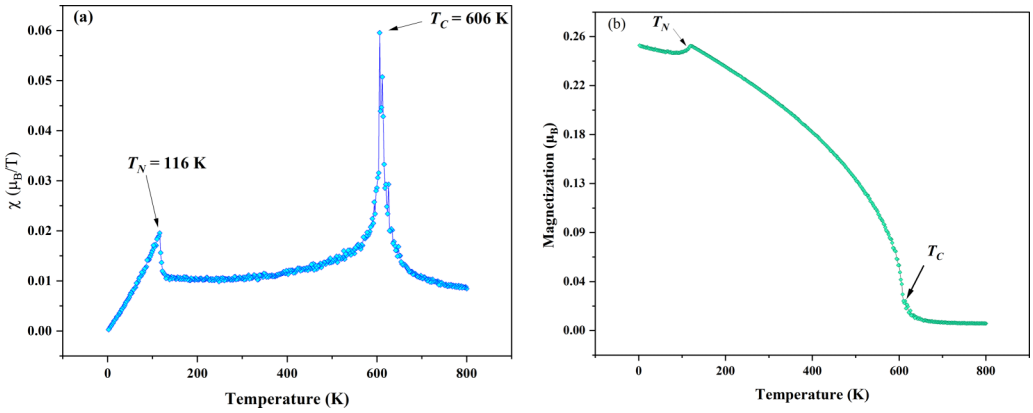


FIG. 13. The complete parameters in the prediction simulation curve. (a) The magnetic susceptibility curve, where the sharp increase of the magnetic susceptibility due to phase change is observed, and the two peaks correspond to the Néel temperature $T_N$ and Curie temperature $T_C$, respectively. (b) The magnetic intensity curve predicted for temperatures up to 800 K.

According to the previously calculated Weiss constant $\theta$ and the formula $f = |\frac{\theta}{T_N}|$, the calculated frustration factor $f = 24.78$, which is significantly $>1$, indicates that the entire system is highly spin frustrating.

## V. CONCLUSIONS

To summarize, in this paper, we first characterized $BiFe_{0.9}Cr_{0.1}O_3$ by XRD and Mössbauer spectroscopy. Its magnetism and the charge distribution around Fe atoms have been investigated in a relatively complex structural system, and the $M$ vs $H$ curve exhibits weak coercivity and high saturation magnetization. The PSO algorithm is used to find the Heisenberg model parameters that best fit the experimental data. However, the effect of the first attempt at single-phase fitting is not favorable. The analysis results suggested the possibility of $Fe^{3+}$-O-$Cr^{3+}$ AFM superexchange. By establishing a two-phase Heisenberg model (cubic structure and relaxation structure), more appropriate fitting parameters are obtained, as well as the ratio of relaxation structure to cubic structure. As determined by the obtained parameters, the more precise Néel temperature is ∼116 K, and the phase transformation temperature from FM to paramagnetic is predicted to be ∼606 K. This suggests that the system is in a state of high spin frustration.

## ACKNOWLEDGMENTS

This paper was supported partly by National Natural Science Foundation of China (Grant No. 12105137), the Natural Science Foundation of Hunan Province, China (Grant No. 2020JJ4517), Research Foundation of Education Bureau of Hunan Province, China (Grant No. 19C1621, 19A434), the National Undergraduate Innovation and Entrepreneurship Training Program Support Projects of China (Grant No. 20200112).

[1] J. Wang, Y. Wei, J. Zhang, L. Ji, Y. Huang, and Z. Chen, Synthesis of pure-phase $BiFeO_3$ nanopowder by nitric acid-assisted gel, Mater. Lett. **124**, 242 (2014).

[2] A. Navrotsky, Energetics and crystal chemical systematics among ilmenite, lithium niobate, and perovskite structures, Chem. Mater. **10**, 2787 (1998).

[3] V Sharma, R. K Ghosh, and B. K Kuanr, Investigation of room temperature ferromagnetism in transition metal doped $BiFeO_3$, J. Phys.: Condens. Matter **31**, 395802 (2019).

[4] H. C. Verma, Preparation, structural and magnetic studies on $BiFe_{1-x}Cr_xO_3$ ($x = 0.0$, 0.05 and 0.1) multiferroic nanoparticles, AIP Adv. **3**, 032140 (2013).

[5] J. K. Kim, S. S. Kim, W. J. Kim, A. S. Bhalla, and R. Guo, Enhanced ferroelectric properties of Cr-doped $BiFeO_3$ thin films grown by chemical solution deposition, Appl. Phys. Lett. **88**, 132901 (2006).

[6] I. Sosnowska, T. Peterlin-Neumaier, and E. Steichele, Spiral magnetic ordering in bismuth ferrite, J. Phys. C **15**, 4835 (1982).

[7] P. Baettig and N. A. Spaldin, *Ab initio* prediction of a multiferroic with large polarization and magnetization, Appl. Phys. Lett. **86**, 012505 (2005).

[8] V. S. Pokatilov, V. S. Rusakov, A. S. Sigov, and A. A. Belik, Mössbauer studies of multiferroics $BiFe_{1-x}Cr_xO_3$ ($x = 0$–0.20), Phys. Solid. State **59**, 1558 (2007).

[9] Z. Xiong and L. Cao, Tailoring morphology, enhancing magnetization and photocatalytic activity via Cr doping in $Bi_{25}FeO_{40}$, J. Alloy Compd. **773**, 828 (2019).

[10] W. Song and B. Liu, Electronic structure and magnetic and optical properties of double perovskite $Bi_2FeCrO_6$ from first-principles investigation, Chinese Phys. B **22**, 047506 (2013).

[11] P. Baettig, C. Ederer, and N. A. Spaldin, First principles study of the multiferroics $BiFeO_3$, $Bi_2FeCrO_6$, and $BiCrO_3$: Structure, polarization, and magnetic ordering temperature, Phys. Rev. B **72**, 214105 (2005).

[12] M. R. Suchomel, C. I. Thomas, M. Allix, M. J. Rosseinsky, and A. M. Fogg, High pressure bulk synthesis and characterization of the predicted multiferroic $Bi(Fe_{1/2}Cr_{1/2})O_3$, Appl. Phys. Lett. **90**, 112909 (2007).

[13] Y. Yüksel, Monte Carlo simulation of Prussian blue analogs described by Heisenberg ternary alloy model, J. Phys. Chem. Solids **86**, 207 (2015).

[14] A. K. Sinha, B. Bhushan, Jagannath, R. K. Sharma, S. Sen, B. P. Mandal, S. S. Meena, P. Bhatt, C. L. Prajapat, A. Priyam, S. K. Mishra, and S. C. Gadkari, Enhanced dielectric, magnetic and optical properties of Cr-doped $BiFeO_3$ multiferroic nanoparticles synthesized by sol-gel route, Results Phys. **13**, 102299 (2019).

[15] S. S. Arafat, Structural transition and magnetic properties of high Cr-doped $BiFeO_3$ ceramic, Cerâmica **66**, 114 (2020).

[16] F. Chang, N. Zhang, F. Yang, S. Wang, and G. Song, Effect of Cr substitution on the structure and electrical properties of $BiFeO_3$ ceramics, J. Phys. D Appl. Phys. **40**, 7799 (2007).

[17] I. P. Raevski, S. P. Kubrin, A. V. Pushkarev, N. M. Olekhnovich, Y. V. Radyush, V. V. Titov, M. A. Malitskaya, S. I. Raevskaya, and H. Chen, The effect of Cr substitution for Fe on the structure and magnetic properties of $BiFeO_3$ multiferroic, Ferroelectrics **525**, 1 (2018).

[18] C. Tabares-Muñoz, J. P. Rivera, A. Bezinges, A. Monnier, and H. Schmid, Measurement of the quadratic magnetoelectric effect on single crystalline $BiFeO_3$, Jpn. J. Appl. Phys. **24**, 1051 (1985).

[19] J. R. Teague, R. Gerson, and W. J. James, Dielectric hysteresis in single crystal $BiFeO_3$, Solid State Commun. **8**, 1073 (1970).

[20] D. Lebeugle, D. Colson, A. Forget, M. Viret, P. Bonville, J. F. Marucco, and S. Fusil, Room temperature coexistence of large electric polarization and magnetic order in $BiFeO_3$ single crystals, Phys. Rev. B **76**, 024116 (2007).

[21] M. Ncube, D. Naidoo, K. Bharuth-Ram, D. Billing, H. Masenda, D. R. Sahu, B. K. Roul, and R. M. Eramus, XRD and Mössbauer spectroscopy study of Ho doped $BiFeO_3$, Hyperfine Interact. **219**, 83 (2013).

[22] N. N. Greenwood and T. C. Gibb, *Mössbauer Spectroscopy* (Chapman and Hall, London, 1971).

[23] A. R. Makhdoom, M. J. Akhtar, M. A. Rafiq, M. Siddique, M.

Iqbal, and M. M. Hasan, Enhancement in the multiferroic properties of $BiFeO_3$ by charge compensated aliovalent substitution of Ba and Nb, AIP Adv. **4**, 037113 (2014).

[24] A. V. Zalesskii, A. A. Frolov, A. Khimich, and A. A. Bush, Composition-induced transition of spin-modulated structure into a uniform antiferromagnetic state in a $Bi_{1-x}La_xFeO_3$ system studied using $^{57}$Fe NMR, Phys. Solid State. **45**, 141 (2003).

[25] V. S. Pokatilov, V. V. Pokatilov, and A. S. Sigov, Local states of iron ions in multiferroics $Bi_{1-x}La_xFeO_3$, Phys. Solid State. **51**, 552 (2009).

[26] V. S. Rusakov, V. S. Pokatilov, A. S. Sigov, M. E. Matsnev, and T. V. Gubaidulina, Diagnostics of a spatial spin-modulated structure using nuclear magnetic resonance and Mössbauer spectroscopy, JETP Lett. **100**, 463 (2014).

[27] P. A. Joy, P. S. Anil Kumar, and S. K. Date, The relationship between field-cooled and zero-field-cooled susceptibilities of some ordered magnetic systems, J. Phys.: Condens. Matter **10**, 11049 (1998).

[28] J. B. Goodenough, *Magnetism and the Chemical Bond* (Wiley, New York, 1963).

[29] S. Kazan, F. A. Mikailzade, M. Özdemir, B. Aktaş, B. Rameev, A. Intepe, and A. Gupta, Ferromagnetic resonance in double perovskite epitaxial thin films of $La_2NiMnO_6$ on $SrTiO_3$ and $NdGaO_3$ substrates, Appl. Phys. Lett. **97**, 072511 (2010).

[30] A. Jaiswal, R. Das, K. Vivekanand, P. M. Abraham, S. Adyanthaya, and P. Poddar, Effect of reduced particle size on the magnetic properties of chemically synthesized $BiFeO_3$ nanocrystals, J. Phys. Chem. C. **114**, 2108 (2010).

[31] S. V. Vijayasundaram, G. Suresh, and R. Kanagadurai, Synthesis, thermal, structural, and magnetic properties of phase-pure nanocrystalline $BiFeO_3$ via wet chemical route, Appl. Phys. A **121**, 681 (2015).

[32] P. V. Midhunlal, J. A. Chelvane, D. Prabhu, R. Gopalan, and N. H. Kumar, $Mn_2V_{0.5}Co_{0.5}Z$(Z = Ga, Al) Heusler alloys: High $T_c$ compensated *p*-type ferrimagnetism in arc melted bulk and *n*-type ferrimagnetism in melt-spun ribbons, J. Magn. Magn. Mater. **489**, 165298 (2019).

[33] L. Dzyaloshinsky, A thermodynamic theory of "weak" ferromagnetism of antiferromagnetics, J. Phys. Chem. Solids. **4**, 241 (1957).

[34] T. Moriya, Anisotropic superexchange interaction and weak ferromagnetism, Phys. Rev. **120**, 91 (1960).

[35] R. Mazumder, P. S. Devi, D. Bhattacharya, P. Choudhury, and A. Sen, Ferromagnetism in nanoscale $BiFeO_3$, Appl. Phys. Lett. **91**, 062510 (2007).

[36] T. Karan and S. Ram, Lattice strain and ferromagnetism in pure and substituted $BiFeO_3$ samples, AIP Conf. Proc. **1536**, 971 (2013).

[37] R. Nechache, C. Nauenheim, U. Lanke, A. Pignolet, F. Rosei, and A. Ruediger, Coexistence of antiferromagnetic and ferromagnetic orders at remanent state in epitaxial multiferroic $Bi_2FeCrO_6$ nanostructures, J. Phys.: Condens. Matter **24**, 142202 (2012).